# Interfacial Fluid Rheology of Soft Particles

Maximilian M. Schmidt,[1] José Ruiz-Franco,[2] Steffen Bochenek,[1] Fabrizio Camerin,[3] Emanuela Zaccarelli,[4,5,*] and Andrea Scotti[6,†]

[1]*Institute of Physical Chemistry, RWTH Aachen University, Landoltweg 2, 52074 Aachen, Germany*
[2]*Laboratory of Physical Chemistry and Soft Matter, Wageningen University & Research, Stippeneng 4, 6708 WE Wageningen, The Netherlands*
[3]*Soft Condensed Matter & Biophysics, Debye Institute for Nanomaterials Science, Utrecht University, Princetonplein 1, 3584 CC Utrecht, The Netherlands*
[4]*Italian National Research Council—Institute for Complex Systems (CNR-ISC), Sapienza University of Rome, Piazzale Aldo Moro 5, 00185 Rome, Italy*
[5]*Department of Physics, Sapienza University of Rome, Piazzale Aldo Moro 2, 00185 Rome, Italy*
[6]*Department of Biomedical Science, Faculty of Health and Society, Malmö University, SE-205 06 Malmö, Sweden*

(Received 9 May 2023; revised 18 August 2023; accepted 20 November 2023; published 22 December 2023)

*In situ* interfacial rheology and numerical simulations are used to investigate microgel monolayers in a wide range of packing fractions, $\zeta_{2D}$. The heterogeneous particle compressibility determines two flow regimes characterized by distinct master curves. To mimic the microgel architecture and reproduce experiments, an interaction potential combining a soft shoulder with the Hertzian model is introduced. In contrast to bulk conditions, the elastic moduli vary nonmonotonically with $\zeta_{2D}$ at the interface, confirming long-sought predictions of reentrant behavior for Hertzian-like systems.

DOI: 10.1103/PhysRevLett.131.258202

Although softness is a concept used in everyday life, its impact on the macroscopic response of a material is still far from being fully understood [1]. Colloidal suspensions are fundamental model systems used to investigate phase transitions and the behavior of complex fluids [2–4]. Polymer-based colloids, particularly microgels [5], allow us to investigate the effect of particle compressibility [6] on fundamental problems such as crystallization [7–9], glass transition [10–13], and flow of non-Newtonian fluids [14–17]. Microgels have also been employed to investigate crystallization in 2D [18–21]. In fact, they spontaneously adsorb at interfaces reducing the interfacial tension between two liquids, undergoing a strong deformation and enhanced stretching [22]. They can be considered a model system for soft particles with nonhomogeneous compressibility, due to their underlying core-corona structure [23,24], allowing us to introduce particle softness in the study of the phase behavior and flow properties in the two-dimensional interfacial plane.

Several recent *ex situ* experimental observations have reported that microgels crystallize in hexagonal lattices and undergo a solid-to-solid transition with increasing concentration [25,26]. The structure of the monolayer has also been addressed *in situ* [27,28], where important differences have been observed with respect to *ex situ* measurements. It thus appears fundamental to address the properties of the monolayer by *in situ* techniques [29,30] and by appropriate theoretical modeling [22,31,32].

Here, poly(*N*-isopropylacrylamide) (pNIPAM) microgels are confined at the oil-water interface and their flow properties are investigated *in situ*. To this aim, amplitude and frequency sweeps, as well as flow curves, are measured using a rheometer with a custom-made double wall-ring accessory and a purpose-built Langmuir trough [30,33]. We measure both the storage modulus and the apparent yield stress of the monolayer and find that they undergo a nonmonotonic variation with increasing generalized packing fraction. This is in contrast to what is observed in bulk [12,34,35], where higher particle density leads to a monotonic increase of these quantities [12,36,37].

Experiments are supported by computer simulations in equilibrium, based on a coarse-grained model where a soft shoulder complements the Hertzian interaction (SSH potential), capturing the main features of the monolayer phase behavior. This model is further used to simulate the flow of the monolayer, confirming the nonmonotonicity of the yield stress with increasing particle density. Finally, we relate the flow behavior to the different regimes of the compression isotherms and identify the onset of two different master curves. Our results highlight the impact of particle softness on the flow of the monolayer and the importance of inhomogeneous compressibility, which gives rise to multiple and unusual rheological regimes in ultradense conditions.

We perform experiments on 5 mol% cross-linked microgels at an oil-water interface at 20 °C. In Fig. 1, we report the compression isotherms of the microgels at the interface as a function of their interfacial generalized packing fraction $\zeta_{2D}$, which corresponds to the area occupied by

 

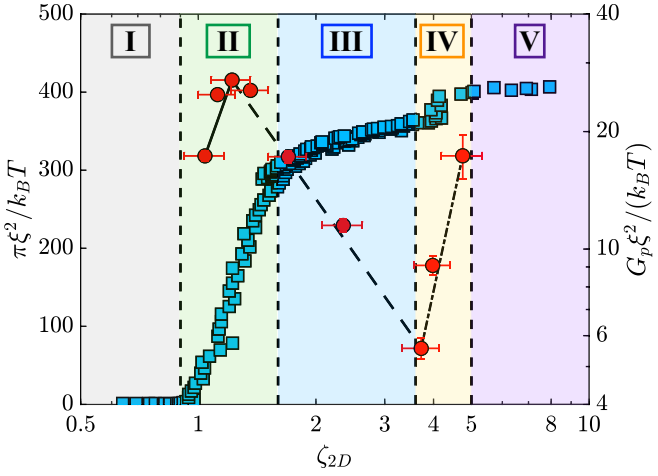


FIG. 1. Compression isotherms reporting the surface pressure $\pi$ (squares) and plateau of the elastic modulus $G_p$ (circles), normalized by $k_BT/\xi^2$, as a function of generalized packing fraction $\zeta_{2D}$. Lines are guides to the eye. Different colors identify different regimes of the compression isotherms.

the microgels using their interfacial radius in the dilute limit $R_{2D} \sim 350$ nm [see Supplemental Material (SM) [38] Eq. (S1)]. This is estimated using atomic force microscopy (AFM) images of isolated microgels (Fig. S1) [1,23]. The surface pressure $\pi$ vs $\zeta_{2D}$ behavior is consistent with previous measurements [1,25,39], which have identified five regimes corresponding to different compressions of the particles and to the formation of hexagonal lattices with different nearest neighbor distances (NND) [25]; see Figs. S2–S4.

To understand how the compression of the microgels affects the elasticity of the monolayer, *in situ* oscillatory frequency sweeps were performed in the linear viscoelastic regime (Fig. S5) to measure the variation of the storage $G'$ and loss $G''$ interfacial moduli (Fig. S7). For all measured $\zeta_{2D}$, the monolayer can be considered a solid with $G' > G''$. While $G'$ remains almost constant, $G''$ shows a local minimum at a characteristic frequency $\omega_m$. This behavior is consistent with the corresponding bulk measurements for microgel suspensions in the glassy state [12,34]. Conventionally, the plateau of the elastic modulus $G_p$ is defined as $G_p = G'(\omega_m)$ [12].

In bulk (3D), $G_p^{3D}$ is usually normalized by the characteristic modulus associated with entropic elasticity $k_BT/R_h^3$, where $k_B$ is the Boltzmann constant, $T$ the temperature, and $R_h$ the hydrodynamic radius of the particles [12,36,37]. Such a normalization gives one an idea of the relation between the internal energy of the system and the thermal fluctuations. If $G_p^{3D} \gg k_BT/R_h^3$, thermal fluctuations are negligible and the physics determining the properties of the suspension is related to the particle deformation or interpenetration with its neighbors [34,40–42]. At the interface, we can perform a similar normalization using the ratio between $k_BT$ and the square of an appropriate characteristic length. The particle radius is a natural first choice, but in the present study it always leads to $G_p \gg k_BT/R_h^2$, even at the lowest studied packing fraction, where the system is already a solid in the form of a hexagonal crystal [25]. This suggests that thermal fluctuations are always irrelevant for the monolayer and that its overall elastic properties are controlled by length scales much smaller than the particle size. Indeed, by considering the mesh size of the microgels ($\xi \approx 10$ nm) [6] as the characteristic length, we obtain $G_p\xi^2/k_BT \approx 1$. This means that the elasticity of the monolayer is mainly determined by the capability of the particles to stretch at the interface, which is related to the deformability of the network, expressed by $\xi$ [1].

In Fig. 1 (right $y$ axis), the normalized values of $G_p$ are plotted as a function of $\zeta_{2D}$. In contrast to that observed in bulk [8,10,34], the evolution of $G_p$ with $\zeta_{2D}$ is nonmonotonic. In particular, $G_p$ (circles) grows during regimes II and IV ($1.0 \lesssim \zeta_{2D} \lesssim 1.6$ and $3.6 \lesssim \zeta_{2D} < 5.0$), while it decreases in regime III, in correspondence of the plateau of the measured compression isotherms (squares). Regimes II and IV correspond to the compression of regions of the microgels with different softness (external corona and core) [6,43]. Figure S3 shows the values of the NND obtained from the analysis of AFM micrographs in dry state (Fig. S2). The values of NND vary as $\zeta^{-1/2}$ (solid line) in regime II (circles), as expected for particles interacting via soft repulsive potentials. To provide a microscopic interpretation of the nonmonotonic behavior of $G_p$, we first note that in region II, the coronas of the microgels are still partially swollen, but the compression of the monolayer progressively compacts them. However, until region III is reached, there is no microgel for which the corona is completely collapsed, with others still retaining a partial swollen corona (see AFM micrographs in Fig. S2). From the AFM images, it seems that particles with a collapsed corona form clusters, Fig. S2. However, recent studies have shown that the presence of clusters might be due to the monolayer deposition on a solid substrate [27,28]. Independently of the presence of the clusters, the key aspect that characterizes regime III is that there are three different kinds of contact between microgels: (i) partially compressed corona-partially compressed corona; (ii) partially compressed corona-core; (iii) core-core (with potential presence of clusters). Thus, under these conditions, the monolayer has a more heterogeneous structure with core-core contacts continuously replacing corona-corona ones. This determines a less efficient transmission of the stress throughout the system, that we attribute to the fact that corona-corona contacts would ensure a higher degree of connectivity within the monolayer as compared to hard core contacts. This effect results in a decrease of $G_p$. We further note that, if the clusters are present, they might also play a role in the decrease of $G_p$, similarly to that reported for depletion gels [44–46]. The following rise of $G_p$ in

region IV is caused by a further increase of the packing fraction $\zeta_{2D}$ that brings the cores in closer and closer contact.

To probe the effect of softness on the flow of the microgel monolayer, we measured the flow curves at different $\zeta_{2D}$, Fig. S8. These curves can be described by $\sigma(\dot{\gamma}) = \sigma_y + k\dot{\gamma}^u + k'\dot{\gamma}^p$, where $\dot{\gamma}$ is the shear rate, $\sigma_y$ is named (apparent) yield stress by analogy to solids, $k$ and $k'$ are fitting parameters, and $u$ and $p \in \mathbb{R}$ and are empirical parameters [47,48]; see Fig. S9 and SM [38] for more details. This is the same functional form used to fit flow curves of concentrated microgel suspensions in bulk [12,37]. In the inset of Fig. 2, the triangles show the variation of $\sigma_y$ normalized by $k_BT/\xi^2$ as a function of $\zeta_{2D}$. The behavior of $\sigma_y$ is similar to that observed for $G_p$ in Fig. 1(a), spanning an increase of roughly one order of magnitude upon initial compression, and undergoing a nonmonotonic behavior at larger values of $\zeta_{2D}$. Interestingly, both $\sigma_y$ and $G_p$ do not show an overall increase between the lowest and highest studied $\zeta_{2D}$, suggesting that within the explored range of packing fractions, the system does not reach a jammed state, according to the definition of Ref. [12].

After associating the different regimes of the compression isotherms with the nonmonotonic response of $G_p$, we question whether this behavior affects the rheological response of the microgels at the interface under flow. To this aim, it is essential to define a unified scale that enables

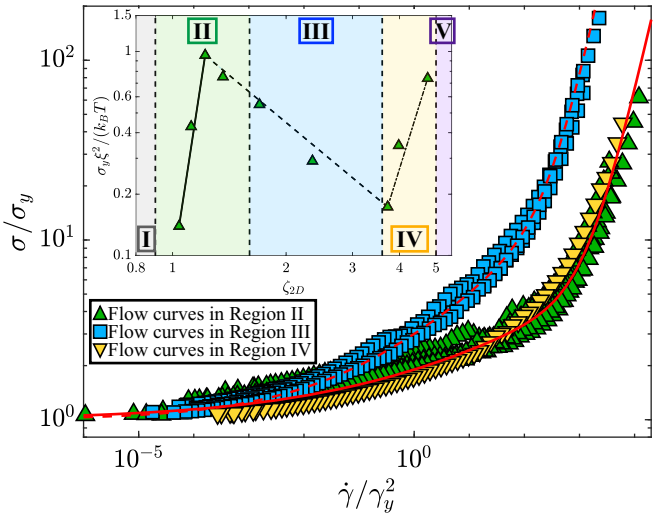


FIG. 2. Master curves obtained by the flow curves measured in the different compression stages where the stress $\sigma$ is normalized by the apparent yield stress $\sigma_y$ and the shear rate $\dot{\gamma}$ is normalized by $\gamma_y^2$, where $\gamma_y^2$ is the threshold strain amplitude between liquidlike and solidlike behavior. Solid and dashed lines correspond to $\sigma/\sigma_y = 1 + k(\gamma/\gamma_y^2)^u + k'(\gamma/\gamma_y^2)^p$ with $p \simeq 0.2$ and $u \simeq 1.1$ and $p \simeq 0.3$ and $u \simeq 1.65$, respectively. Inset: $\sigma_y$, normalized by $k_BT/\xi^2$ as a function of the generalized area fraction, $\zeta_{2D}$. The different regimes of the compression isotherms in Fig. 1 are indicated by different colors.

the evaluation of the flow behavior across different regimes and $\dot{\gamma}$. Following Cloitre and coworkers [12,49], we plot $\sigma/\sigma_y$ vs $\dot{\gamma}/\gamma_y^2$, where $\gamma_y \propto \sigma_y/G_p$ [49]. The values of $\gamma_y$ and the corresponding errors have been determined by fitting the two different slopes of the flow curves measured in the amplitude sweeps (Fig. S5). As shown in Fig. S6(a), $\gamma_y$ rapidly increases in regime II before reaching a plateau in regime III, and then decreasing in regime IV. Through this analysis, Fig. 2 shows two distinct master curves: the first one roughly corresponds to the monolayer in regimes II and IV (triangles), while the second to regime III (squares) of the compression isotherm. The normalization by $1/\gamma_y^2$ is fundamental to obtain two well distinct master curves between regimes II/IV and III, as shown in Fig. S6(b).

To shed light on the particle-to-particle interactions that give rise to this behavior, we introduce a novel interaction potential. This is needed since a simple 2D Hertzian model, shown in Fig. 3(a), is too soft and fails to reproduce the behavior of the moduli at high $\zeta_{2D}$, as well as the evolution of NND with compression, see Fig. S3. We thus complement the Hertzian, which works very well up to regime II, with a square shoulder potential [50,51], mimicking the presence of a stiffer core, as illustrated in Fig. 3(a). This also highlights the three characteristic lengths of the SSH model: the compressible corona, dominating at low and intermediate $\zeta_{2D}$, the standard core, e.g. determined by the fuzzy sphere model where the square shoulder takes over from the Hertzian, and, finally, an incompressible core, emerging at very large packing fractions due to the fact that the smallest value of the NND does not decrease any further. Simulations with the SSH model, also accounting for the experimental size polydispersity, are able to quantitatively reproduce the behavior of NND for both lengths, as a function of $\zeta_{2D}$, as shown in Figs. S3 and S10 to S12.

We then perform simulations of the monodisperse 2D Hertzian and of the polydisperse SSH models under steady shear (details in the SM [38]). For each studied shear rate $\dot{\gamma}$ and $\zeta_{2D}$, the mean value of the shear stress $\sigma_{xy}$ at the steady state is extracted. The resulting flow curves (Fig. S13) are well described by the standard Herschel-Bulkley model, i.e., $\sigma(\dot{\gamma}) = \sigma_y + k\dot{\gamma}^u$. Figure 3(b) reports the yield stress $\sigma_y$ obtained from the fits of the simulated flow curves, normalized by the maximum of $\sigma_y$ for $\zeta_{2D} \sim 5.5$, that is the maximum packing fraction probed in the experiments. For the Hertzian model, we observe a transition from a Newtonian fluid at low $\zeta_{2D}$ in regime I to a viscoelastic response with a nonmonotonic behavior of $\sigma_y$ in regime II, before recovering a fluid behavior at higher area fractions. This reentrant behavior is a well-known hallmark for static and dynamic properties of Hertzian systems [22,52,53], but to our knowledge it was not previously reported for elastic properties.

For the SSH model, we find an almost identical qualitative behavior to the Hertzian up to regime III, that is then followed by a second growth of $\sigma_y$ in regime V.

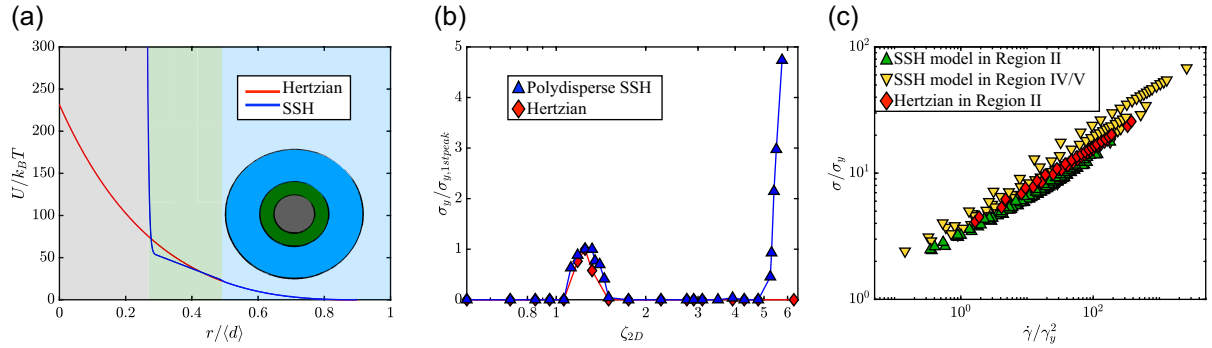


FIG. 3. (a) Comparison between the 2D Hertzian potential (red curve) and the square-shoulder Hertzian model (SSH) (blue curve), where we highlight the three different regions of the particle: corona (light blue), compressible core (green), and incompressible core (gray). Corresponding colors are used in the background of the panel; (b) apparent yield stress $\sigma_y$ normalized to the values of the first maximum of $\sigma_y$ ($\sigma_{y,1\mathrm{stpeak}}$) as a function of $\zeta_{2D}$; (c) scaling flow curves, $\sigma/\sigma_y$ vs $\dot{\gamma}/\gamma_y^2$, obtained from simulations using the monodisperse Hertzian (diamonds) and the polydisperse SSH (triangles) potential.

The deviations between experiments and simulations in regimes III and IV (see Fig. 2) are likely due to the coarse-grained nature of the model, which does not incorporate key polymeric aspects of the microgels. Indeed, it can be seen also in the experiments that the difference between $G'$ and $G''$ in regime III is smaller (see Figs. S5 and S7), but the system remains solidlike probably because of entanglements between the coronas, a feature that cannot be captured by a simple point-particle model such as the present one. This difference may also explain the fact that the growth of $\sigma_y$ only occurs in regime V, rather than already in regime IV as in experiments, confirming the overall tendency of the simulations to retain a more fluidlike behavior than the experiments. Nonetheless, the reincrease of $\sigma_y$ observed at larger $\zeta_{2D}$ is well captured by the model, thanks to the presence of the inner core in the SSH model. The comparison of the behavior of $\sigma_y$ with that of the mean-squared displacement (Fig. S12) demonstrates that the nonmonotonicity of the moduli is the manifestation of such reentrant behavior in the elastic properties of the system.

We also analyze the scaling of the flow curves in simulations, using the same normalization applied to the experimental data in Fig. 2. The plot reported in Fig. 3(c), although spanning a smaller range than experiments, indicates that data in regimes II and IV/V roughly belong to the same master curve. Therefore, the behavior of the flow curves and the variation of $\sigma_y$ with $\zeta_{2D}$ confirm that regimes II and IV/V are similar in terms of their flow and elastic properties. The rescaled flow curves obtained using the Hertzian model are also reported in Fig. 3(c), being almost indistinguishable from those of the SSH model up to regime II. This confirms that before the corona compression, the interaction between microgels can be approximated with a simple Hertzian model, as predicted from numerical calculations of the effective potentials in the dilute limit [22].

In summary, we reported interfacial rheology measurements of monolayers of soft microgels at an oil-water interface. The experiments are compared to numerical simulations where a Hertzian is combined with a square shoulder potential, based on the core-corona structure of the microgels [43]. We find the onset of a nonmonotonic behavior of the elastic moduli with increasing packing fraction due to the Hertzian contribution that is dominant at not too large packing fractions. Hence, after an initial fluid behavior (regime I), the system becomes viscoelastic (regime II), but the moduli start to decrease again (regime III), until a second increase is observed at very large $\zeta_{2D}$ (regimes IV and V). Simulations with such interaction potential qualitatively capture these features, except for the solidlike character of regime III.

The nonmonotonic dependence of the moduli on packing fraction can also be interpreted in terms of the energy of the system: when particles have comparable softness, either before the microgel coronas start to be significantly compressed, or after the microgels make core-core contacts, the monolayer stores energy with increasing $\zeta_{2D}$. The similarity between regime II and IV/V is further supported by the behavior of their flow curves, which are reduced to the same master curve. However, a different behavior (and associated master curve) applies in regime III, where the monolayer dissipates energy. This coincides with the onset of a second characteristic nearest neighbor distance in the radial distribution functions, highlighted by a plateau in the compression isotherms and denoting the emergence of core-core interactions. In this region, the contacts between particles are of different kinds, being either corona-corona, corona-core, or core-core. Such heterogeneities in the monolayer structure, and the different types of contacts between particles with different softness, decrease the transmission of the stress through the interface leading to the observed decrease in $G_p$. These findings indicate the ability of the microgels to decrease stress thanks to deformation, suggesting that they can effectively reduce the viscous dissipation associated with the compression of their volume, by extending in the aqueous subphase [54].

The present work sheds light on the flow properties of monolayers of soft particle at high concentrations. The fact that the measured elastic moduli do not really exceed those measured at the onset of elasticity suggests that the system does not reach jamming in the investigated range of packing fractions. This can be attributed to the role of individual particle softness and to the additional degrees of freedom of the particles outside the interfacial plane, e.g., through protrusion in the aqueous phase [54]. This peculiar feature of the interfacial behavior of microgels calls for further *in situ* investigations, for example by neutron reflectivity [24] or AFM [29]. These would clarify, for instance, the role of clusters on the flow properties of the monolayer and possible analogies with depletion glasses [44–46], or shed light on the forces leading to cluster formation with possible similarity to the structures formed by proteins and antibodies at interfaces [55,56].

The supporting data for this Letter are openly available [57].

The authors thank M. Brugnoni for the microgel synthesis and W. Richtering, A. Fernandez-Nieves, and M. Cloitre for fruitful discussions. M. M. S., S. B., and A. S. thank the Deutsche Forschungsgemeinschaft within projects A3 and B8 of the SFB 985 Functional Microgels and Microgel Systems. E. Z. acknowledges support from EU MSCA Doctoral Network QLUSTER, Grant Agreement No. 101072964 and ICSC—Centro Nazionale di Ricerca in High Performance Computing, Big Data and Quantum Computing, funded by the European Union—NextGenerationEU-PNRR, Missione 4 Componente 2 Investimento 1.4.

*emanuela.zaccarelli@cnr.it
†andrea.scotti@mau.se

[1] A. Scotti, M. F. Schulte, C. G. Lopez, J. J. Crassous, S. Bochenek, and W. Richtering, Chem. Rev. **122**, 11675 (2022).
[2] V. Trappe, V. Prasad, L. Cipelletti, P. Segre, and D. A. Weitz, Nature (London) **411**, 772 (2001).
[3] A. Duri, D. A. Sessoms, V. Trappe, and L. Cipelletti, Phys. Rev. Lett. **102**, 085702 (2009).
[4] U. Gasser, E. R. Weeks, A. Schofield, P. Pusey, and D. Weitz, Science **292**, 258 (2001).
[5] R. Pelton and P. Chibante, Colloids Surf. **20**, 247 (1986).
[6] J. E. Houston, L. Fruhner, A. de la Cotte, J. Rojo González, A. V. Petrunin, U. Gasser, R. Schweins, J. Allgaier, W. Richtering, A. Fernandez-Nieves *et al.*, Sci. Adv. **8**, eabn6129 (2022).
[7] M. Pelaez-Fernandez, A. Souslov, L. A. Lyon, P. M. Goldbart, and A. Fernandez-Nieves, Phys. Rev. Lett. **114**, 098303 (2015).
[8] A. Scotti, U. Gasser, E. S. Herman, M. Pelaez-Fernandez, J. Han, A. Menzel, L. A. Lyon, and A. Fernández-Nieves, Proc. Natl. Acad. Sci. U.S.A. **113**, 5576 (2016).
[9] J. Ruiz-Franco, J. Marakis, N. Gnan, J. Kohlbrecher, M. Gauthier, M. P. Lettinga, D. Vlassopoulos, and E. Zaccarelli, Phys. Rev. Lett. **120**, 078003 (2018).
[10] J. Mattsson, H. M. Wyss, A. Fernandez-Nieves, K. Miyazaki, Z. Hu, D. R. Reichman, and D. A. Weitz, Nature (London) **462**, 83 (2009).
[11] P. Van Der Scheer, T. Van De Laar, J. Van Der Gucht, D. Vlassopoulos, and J. Sprakel, ACS Nano **11**, 6755 (2017).
[12] C. Pellet and M. Cloitre, Soft Matter **12**, 3710 (2016).
[13] M. J. Bergman, N. Gnan, M. Obiols-Rabasa, J.-M. Meijer, L. Rovigatti, E. Zaccarelli, and P. Schurtenberger, Nat. Commun. **9**, 5039 (2018).
[14] M. E. Helgeson, N. J. Wagner, and D. Vlassopoulos, J. Rheol. **51**, 297 (2007).
[15] S. P. Meeker, R. T. Bonnecaze, and M. Cloitre, Phys. Rev. Lett. **92**, 198302 (2004).
[16] M. Cloitre, R. Borrega, and L. Leibler, Phys. Rev. Lett. **85**, 4819 (2000).
[17] J. Ruiz-Franco, F. Camerin, N. Gnan, and E. Zaccarelli, Phys. Rev. Mater. **4**, 045601 (2020).
[18] S. Deutschländer, T. Horn, H. Löwen, G. Maret, and P. Keim, Phys. Rev. Lett. **111**, 098301 (2013).
[19] B. Illing, S. Fritschi, H. Kaiser, C. L. Klix, G. Maret, and P. Keim, Proc. Natl. Acad. Sci. U.S.A. **114**, 1856 (2017).
[20] A. L. Thorneywork, J. L. Abbott, D. G. A. L. Aarts, and R. P. A. Dullens, Phys. Rev. Lett. **118**, 158001 (2017).
[21] M. Rey, A. D. Law, D. M. A. Buzza, and N. Vogel, J. Am. Chem. Soc. **139**, 17464 (2017).
[22] F. Camerin, N. Gnan, J. Ruiz-Franco, A. Ninarello, L. Rovigatti, and E. Zaccarelli, Phys. Rev. X **10**, 031012 (2020).
[23] A. Scotti, S. Bochenek, M. Brugnoni, M.-A. Fernandez-Rodriguez, M. F. Schulte, J. Houston, A. P. Gelissen, I. I. Potemkin, L. Isa, and W. Richtering, Nat. Commun. **10**, 1418 (2019).
[24] S. Bochenek, F. Camerin, E. Zaccarelli, A. Maestro, M. M. Schmidt, W. Richtering, and A. Scotti, Nat. Commun. **13**, 3744 (2022).
[25] M. Rey, M. Á. Fernández-Rodríguez, M. Steinacher, L. Scheidegger, K. Geisel, W. Richtering, T. M. Squires, and L. Isa, Soft Matter **12**, 3545 (2016).
[26] S. Bochenek, A. Scotti, W. Ogieglo, M. A. Fernandez-Rodriguez, M. F. Schulte, R. A. Gumerov, N. V. Bushuev, I. I. Potemkin, M. Wessling, L. Isa *et al.*, Langmuir **35**, 16780 (2019).
[27] K. Kuk, V. Abgarjan, L. Gregel, Y. Zhou, V. C. Fadanelli, I. Buttinoni, and M. Karg, Soft Matter **19**, 175 (2023).
[28] T. Kawamoto, K. Yanagi, Y. Nishizawa, H. Minato, and D. Suzuki, Chem. Commun. **59**, 13289 (2023).
[29] J. Vialetto, S. N. Ramakrishna, and L. Isa, Sci. Adv. **8**, eabq2019 (2022).
[30] M.-C. Tatry, E. Laurichesse, J. Vermant, V. Ravaine, and V. Schmitt, J. Colloid Interface Sci. **629**, 288 (2023).
[31] S. Ciarella, M. Rey, J. Harrer, N. Holstein, M. Ickler, H. Lowen, N. Vogel, and L. M. Janssen, Langmuir **37**, 5364 (2021).
[32] J. Harrer, S. Ciarella, M. Rey, H. Löwen, L. M. Janssen, and N. Vogel, Soft Matter **17**, 4504 (2021).
[33] S. Vandebril, A. Franck, G. G. Fuller, P. Moldenaers, and J. Vermant, Rheol. Acta **49**, 131 (2010).

[34] G. M. Conley, C. Zhang, P. Aebischer, J. L. Harden, and F. Scheffold, Nat. Commun. **10**, 2436 (2019).
[35] F. Scheffold, P. Díaz-Leyva, M. Reufer, N. Ben Braham, I. Lynch, and J. L. Harden, Phys. Rev. Lett. **104**, 128304 (2010).
[36] A. Ikeda, L. Berthier, and P. Sollich, Soft Matter **9**, 7669 (2013).
[37] A. Scotti, M. Brugnoni, C. G. Lopez, S. Bochenek, J. J. Crassous, and W. Richtering, Soft Matter **16**, 668 (2020).
[38] See Supplemental Material at http://link.aps.org/supplemental/10.1103/PhysRevLett.131.258202 for details on sample preparation and characterisation, rheological and AFM data and additional analysis, and details and additional analysis of simulations data.
[39] K. Geisel, L. Isa, and W. Richtering, Angew. Chem. **126**, 5005 (2014).
[40] G. M. Conley, P. Aebischer, S. Nöjd, P. Schurtenberger, and F. Scheffold, Sci. Adv. **3**, e1700969 (2017).
[41] A. Scotti, A. R. Denton, M. Brugnoni, J. E. Houston, R. Schweins, I. I. Potemkin, and W. Richtering, Macromolecules **52**, 3995 (2019).
[42] T. Höfken, C. Strauch, S. Schneider, and A. Scotti, Nano Lett. **22**, 2412 (2022).
[43] M. F. Schulte, S. Bochenek, M. Brugnoni, A. Scotti, A. Mourran, and W. Richtering, Angew. Chem., Int. Ed. **60**, 2280 (2021).
[44] J. Conrad, H. Wyss, V. Trappe, S. Manley, K. Miyazaki, L. Kaufman, A. B. Schofield, D. Reichman, and D. Weitz, J. Rheol. **54**, 421 (2010).
[45] L. C. Hsiao, R. S. Newman, S. C. Glotzer, and M. J. Solomon, Proc. Natl. Acad. Sci. U.S.A. **109**, 16029 (2012).
[46] K. A. Whitaker, Z. Varga, L. C. Hsiao, M. J. Solomon, J. W. Swan, and E. M. Furst, Nat. Commun. **10**, 2237 (2019).
[47] B. M. Erwin, M. Cloitre, M. Gauthier, and D. Vlassopoulos, Soft Matter **6**, 2825 (2010).
[48] M. Caggioni, V. Trappe, and P. T. Spicer, J. Rheol. **64**, 413 (2020).
[49] J. R. Seth, L. Mohan, C. Locatelli-Champagne, M. Cloitre, and R. T. Bonnecaze, Nat. Mater. **10**, 838 (2011).
[50] M. A. Sandoval-Puentes, A. Torres-Carbajal, A. B. Zavala-Martínez, R. Castañeda-Priego, and J. M. Méndez-Alcaraz, J. Phys. Condens. Matter **34**, 164001 (2022).
[51] E. Jagla, Phys. Rev. E **58**, 1478 (1998).
[52] Z. Zhang, N. Xu, D. T. Chen, P. Yunker, A. M. Alsayed, K. B. Aptowicz, P. Habdas, A. J. Liu, S. R. Nagel, and A. G. Yodh, Nature (London) **459**, 230 (2009).
[53] L. Berthier, A. J. Moreno, and G. Szamel, Phys. Rev. E **82**, 060501(R) (2010).
[54] Y. Gerelli, F. Camerin, S. Bochenek, M. M. Schmidt, A. Maestro, W. Richtering, E. Zaccarelli, and A. Scotti, ChemRxiv, 10.48550/arXiv.2311.08222 (2023).
[55] Y. S. Tein, Z. Zhang, and N. J. Wagner, Langmuir **36**, 7814 (2020).
[56] C. V. Wood, V. I. Razinkov, W. Qi, C. J. Roberts, J. Vermant, and E. M. Furst, Langmuir **39**, 7775 (2023).
[57] M. M. Schmidt *et al.*, RADAR4Chem, 10.22000/1827.